Neutral interstitial iron center in silicon studied by Zeeman spectroscopy

AnnaLena Thilderkvist, Günter Grossmann, Mats Kleverman, and Hermann G. Grimmeiss
Solid State Physics, University of Lund, Box 118, S-221 00 Lund, Sweden
(Received 3 February 1998)

The Zeeman effect of the interstitial iron defect in silicon has been investigated by high-resolution Fourier-transform spectroscopy. Two sets of experimentally observed line spectra have previously been identified as optical excitations of neutral interstitial iron, Fe_i^0. The first set arises when an electron is excited to a shallow-donor-like state, $Fe_i^0 + h\nu \rightarrow Fe^+ + e^-$, where the electron is decoupled from the Fe^+ core whose ground state is a $^4T_1$ term. The second set arises when an excited electron of a_1 symmetry is coupled by exchange interaction to the Fe^+ core, yielding a $^5T_1$ final state. The Zeeman behavior of these transitions is studied in order to verify the assignment of the states and the effective-mass-like character of the decoupled electron. Detailed information on the initial state and on the properties of the iron core is gained. Experiments determine the multiplet splitting of the $^4T_1$ and $^5T_1$ states due to spin-orbit interaction but large deviations from the Landé interval rule are observed, as well as a marked decrease in intensity for the high-energy components. Our analysis confirms that the $^4T_1$ and $^5T_1$ states are closely related, and a dynamical Jahn-Teller distortion is suggested to be the dominant mechanism responsible for the non-Landé behavior. [S0163-1829(98)06036-6]

I. INTRODUCTION

When diffused into the silicon lattice, the transition-metal (TM) impurity iron introduces deep levels in the band gap. In this paper we focus on the isolated interstitial iron defect in silicon, Fe_i, which has been studied by several experimental methods over the years, starting with the classic electron-paramagnetic-resonance (EPR) work of Ludwig and Woodbury (LW).[1] They explained their TM data successfully by what was later to be called the Ludwig-Woodbury model. TM impurities have since then attracted a lot of interest both theoretically[2–4] and experimentally.[3] A basic understanding of these impurities has been gained, mainly based on information derived from EPR measurements which, however, usually probe only the ground state. Transmission experiments on TM defects on the other hand, provide information on the excited states in addition to the ground state. The neutral interstitial TM defect iron in silicon, Fe_i^0, has been shown to give rise to an especially complex absorption spectrum in the range of about 5820–6450 cm^{-1}.[5–8] The excitation spectrum of Fe_i^0 is presented in Ref. 5.

It has been suggested[6] that the transitions in the range 6300–6420 cm^{-1} correspond to excitations of an electron from the ground state of Fe^0 to shallow-donor-like states just below the conduction-band minimum. In the final state of the optical transition, the interaction between the electron in a shallow-donor-like state and the positively charged core was assumed to be negligible. The final state should thus consist of two noninteracting systems, the shallow-donor electron and the residual Fe^+ core, whose ground state is a $^4T_1$ multiplet. It was further reported that the line spectrum consisted of not only one but four series of shallow-donor-like states.[5] This was explained by a shake-up effect where the Fe^+ core, after the optical transition, would be left not only in its lowest ground-state level but also in higher levels of the $^4T_1$ multiplet. The sharp lines in the range 5820–5875 cm^{-1}, labeled Fe_L1 to Fe_L4 in Ref. 5, are also part of the Fe^0 spectrum.[5,8] Here an electron is excited to a more localized a_1 state, which now interacts with the $^4T_1$ core of Fe^+ to form a final state with a $^5T_1$ ground-state term.

In this paper, the interstitial iron center will be analyzed in detail using Zeeman spectroscopy. The electronic structure of the initial ground state and of the two sets of final excited states, $(^4T_1 + e^-)$ and $^5T_1$, are investigated. The common features of the final states in the studied transitions, such as the deviations from the Landé interval rule, and the large decrease in intensity for some higher states, suggest that the final $(^4T_1 + e^-)$ and $^5T_1$ states are closely related.

II. EXPERIMENTAL DETAILS

The samples used in the experimental work were originally *n*-type phosphorus-doped floating-zone silicon with resistivities of 5 and 40 Ω cm. The samples were oriented by x-ray Laue backscattering, and then cut in the three main crystal directions: ⟨100⟩, ⟨110⟩, and ⟨111⟩.

After polishing and cleaning the samples, iron was introduced by means of solid-state diffusion, either by evaporation of iron onto the sample surface or by placing a small iron wire in the quartz ampoule. The sealed quartz ampoules, containing samples, iron, and argon gas at about 300 mbar, were heat treated for approximately 1 h at a temperature of 1260 °C, and then rapidly quenched to room temperature in ethylene glycol. Some of the samples were immediately stored in liquid nitrogen to keep the interstitial iron concentration at a maximum.

The measurements were performed using a BOMEM DA3.01 Fourier-transform spectrometer equipped with a liquid-nitrogen-cooled InSb photodiode detector. In the Zeeman experiments an Oxford Instruments Spectromagnet was used in the Voigt configuration, and spectra were recorded at magnetic fields up to 6.5 T. The sample temperature was 1.9 K. For the annealing experiments a Leybold-Heraeus continuous-flow cryostat was used. The cryostat was cooled

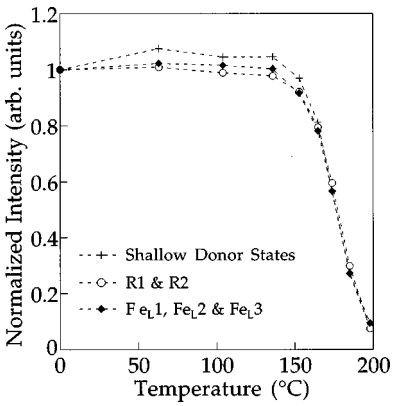

FIG. 1. The annealing behavior of the observed spectral lines in iron doped silicon (see Ref. 5). The annealing was carried out for eight different temperatures between 50 and 200 °C for 30 min. All lines anneal out at about 200 °C.

with liquid helium, and the sample temperature was kept at 10 K.

III. ANNEALING EXPERIMENTS

Annealing of iron diffused into an originally *n*-type silicon sample results in a decrease in intensity of the lines in the range 5820–6420 cm^{-1}. High-resolution spectroscopy measurements combined with photo-EPR have, in an earlier annealing study,[6] identified the line spectra in the range 6300–6420 cm^{-1} to arise from the excitation of Fe_i^0.

Two intense broad lines $R1$ and $R2$ are observed, and further down at 5800–5950 cm^{-1} a series of sharp lines labeled Fe_L1-Fe_L4 are detected.[5] The lowest of these lines is superimposed on a broad line of high intensity. Absorption measurements were carried out after a 30-min anneal at eight temperatures ranging from 50 up to 200 °C. The intensities of the lines Fe_L1, Fe_L2, and Fe_L3 were added and compared to the summed intensities of $R1$ and $R2$ and of the three strongest lines in the shallow-donor series. In Fig. 1, the normalized intensities are plotted versus annealing temperature. We find that Fe_L1, Fe_L2, and Fe_L3 have the same annealing behavior as the lines belonging to the shallow-donor spectra at about 6300 cm^{-1}. The resonance structures $R1$ and $R2$ behave similarly, and all lines are annealed out at a temperature of 200 °C. By inspection of the annealing spectra, it is clear that the broad resonance which peaks at 5800 cm^{-1} anneals out at this same temperature. These experiments strongly suggest that all lines and resonances in the energy range of about 5820–6450 cm^{-1} have the same origin, i.e., the neutral interstitial iron center Fe_i^0.

IV. ELECTRONIC STRUCTURE

Ground state of Fe^0

According to the LW model,[1] the neutral interstitial iron center in silicon has a $t_2^6e^2$ ground-state configuration. The six electrons in the t_2 state form a $^1A_1$ term and the two e electrons form a high-spin $^3A_2$ term, and together a total $^3A_2$ term is formed. Since $S=1$ transforms as T_1 in T_d symmetry, the spin and the orbital part of the $^3A_2$ term may finally be coupled to yield a T_2 level. This model has been verified by EPR measurements, and the g value for the $^3A_2$ ground state of Fe^0 was determined to be $g_{sA}=2.0699$.[1] An effective orbital momentum $1'=1$ can be associated with an electron in the t_2 state, and all matrix elements of the orbital angular momentum operator $\mathbf{L}$ within the t_2 manifold are proportional to those of $\mathbf{L}$ within a manifold of p orbitals $(1=1)$. The single constant of proportionality would assume the value $g_L=-1$ if the t_2 orbitals were pure d orbitals of the iron atom.

Recent calculations[2–4] confirm that interstitial iron indeed gives rise to t_2 and e gap levels, and that Hund's rule is obeyed for the ground state, but the simple LW model has to be modified. The e and t_2 gap states are not pure d like, as expected from the LW model, but contain contributions from both p-like host states and d-like defect states. The nonvanishing matrix elements of $\mathbf{L}$ within the t_2 states are thus expected to be modified by these hybridization effects, and g_L may assume values in the range between 1 and -1, the limiting values corresponding to pure p and pure d orbitals, respectively. The g_L value can be further reduced by covalency and by dynamic Jahn-Teller effects, and experimentally it has been shown to be rather small for $3d$ transition metals in silicon.

The line spectra in the range 6250–6400 cm^{-1} are attributed to transitions where an electron is excited to a shallow-donor state,[5–8] and is thereby effectively removed from the positively charged iron core state Fe^+. The ground state of Fe^+ is a $^4T_1$ term deriving from the $t_2^5e^2$ configuration for the Fe^+ core.[1,2] In a one-particle picture, the transitions thus correspond to exciting an electron from a t_2 orbital to a shallow donor state. Spin-orbit interaction will couple the spin $S=\frac{3}{2}$ to the total effective orbital angular momentum $L'=1$, and the term is split into three levels with effective total angular momentum $J'=\frac{1}{2}$, $\frac{3}{2}$, and $\frac{5}{2}$ transforming as Γ_6, Γ_8, and $\Gamma_7+\Gamma_8$. Again, EPR measurements have shown that $J'=\frac{1}{2}$ is the ground state of Fe^+ with an experimental g value of $g_J=\frac{1}{2}=3.524$.[1]

The delocalization of the shallow-donor states implies that the core of the residual Fe^+ impurity will only weakly interact with the excited electron. In the final state of the transition, the core may then be left in the different levels of the $^4T_1$ multiplet, and we would expect to see three hydrogenic series of donor states corresponding to the three possible values of J'. Effective-mass theory (EMT) can be used to determine the energies within each series, and the three series may be expected to be displaced according to the Landé interval rule, at least within a spherical model, where the $J'=5/2(\Gamma_7,\Gamma_8)$ level remains unsplit.

V. $^4T_1$ CORE PLUS SHALLOW-DONOR STATES

A. Absorption measurements

We will first concentrate on the shallow-donor-like line spectra in the range 6250–6400 cm^{-1}, and then on transitions having final p-like shallow states. The binding energies of the p-like states are rather insensitive to the details of the defect core and should be well given by EMT, since shallow-donor states are delocalized and p-like states have a node at the origin. Silicon has six equivalent conduction-band minima along the [100] directions, and this implies that all

TABLE I. The experimental energies of the *p*-like shallow donor states of the four series *A*, *B*, *C*, and *D*. All energies are given in wave numbers (cm^{-1}). The energies given in parentheses are the corresponding binding energy of each state, obtained by assuming that the $2p_{\pm}$ state of each series is given exactly by EMT. The EMT binding energies of each state, obtained from a variational calculation (Ref. 10), are given in the last column.

Final state	Series *A*	Series *B*	Series *C*	Series *D*	EMT
$2p_0$	6268.61	6310.83	6318.73	6324.34	
	(92.75)	(92.66)	(92.80)	(92.88)	(92.69)
$2p_{\pm}$	6309.72	6351.85	6359.89	6365.58	
	(51.64)	(51.64)	(51.64)	(51.64)	(51.64)
$3p_0$	6317.11	6359.34	6367.20	6372.95	
	(44.25)	(44.15)	(44.33)	(44.27)	(44.24)
$4p_0$	6334.55	6376.68		6390.42	
	(26.81)	(26.81)		(26.80)	(26.69)
$3p_{\pm}$	6336.11	6378.20	6386.2	6391.88	
	(25.25)	(25.29)	(25.3)	(25.34)	(25.16)
$4p_{\pm}$	6343.61	6385.74		6399.37	
	(17.75)	(17.75)		(17.85)	(17.64)
$5p_{\pm}$	6349.37	6391.88			
	(11.99)	(11.61)			(11.69)
E_B^i	6361.36	6403.49	6411.53	6417.22	
$E_B^i - E_B^A$	0	42.13	50.16	55.86	

donor states are at least sixfold degenerate in a first single-valley approximation. In T_d symmetry p_0 states transform as A_1+E+T_2, whereas the $p_{\pm}$ states transform as $2T_1+2T_2$. The valley-orbit interaction and central-cell effects lift this accidental degeneracy.

The electric dipole operator has T_2 symmetry. The Fe^0 ground state has a $t_2^6e^2$ configuration, and when an electron is excited from the t_2 shell, optical dipole transitions are allowed to all one-particle states having transformation properties which appear in the reduction of the direct product $T_2\times T_2\rightarrow A_1+E+T_1+T_2$. Although symmetry considerations thus allow transitions to all valley-orbit-split states, they give no information on their relative intensities, for which we would need to evaluate the corresponding transition matrix elements.

The four different series of shallow donor spectra are attributed to the energy-level structure of the Fe^+ core.[5] The ground state of the $^4T_1$ multiplet is the $J'=\frac{1}{2}$ level, which we thus associate with the line series observed at the lowest excitation energy, labeled *A*. The second series, labeled *B*, we accordingly attribute to the $J'=\frac{3}{2}$ Fe^+ core level. The third and fourth series are labeled *C* and *D*. Since the $J'=\frac{5}{2}$ state is expected to split in a nonspherical environment, the *C* and *D* series could be explained by the two final-state components of the $J'=\frac{5}{2}$ level with symmetric Γ_7 and Γ_8, respectively.

In Table I, the energies of the identified lines from the *A*, *B*, *C*, and *D* series are given. Taking the $2p_{\pm}$ line in each series as reference, we have determined the ionization limit for all four series. The $J'=\frac{3}{2}$ level is found to lie 42.1 cm^{-1} above $J'=\frac{1}{2}$. The Landé interval rule then predicts the $J'=\frac{5}{2}$ level to lie $\frac{5}{3}\times 42.1\ cm^{-1}$ above the $J'=\frac{3}{2}$ level. No spectral features, however, appear in this energy range. On the other hand, it is tempting to associate the *C* and *D* series found 8.1 and 13.8 cm^{-1} above the $J'=\frac{3}{2}$ level with the two split components Γ_7 and Γ_8 of the $J'=\frac{5}{2}$ level. In this case, however, the splitting of the $^4T_1$ multiplet would deviate significantly from the Landé interval rule.

B. Zeeman spectroscopy

In a magnetic field the line spectra involving transitions to shallow-donor-like states show a very complicated splitting pattern. To account for this behavior, we must superimpose the Zeeman behavior of the initial $^3A_2$ Fe^0 state, of the final $^4T_1$ core, and of the shallow-donor states. The behavior of the initial state is well known from EPR measurements, and the Zeeman behavior of shallow-donor states, is treated in detail in Ref. 9. In order to account for the splitting of the Fe^+ core, we need to have a better understanding of the large deviations from the Landé interval rule. We postpone a discussion of the Zeeman effect for these states until Sec. VIII, when a more detailed analysis of the overall behavior of the Fe_i center is carried out. We first turn to an analysis of the final $^5T_1$ state.

VI. $^5T_1$ EXCITED STATE

In order to determine the origin of the three sharp lines Fe_L1-Fe_L3 in the range from 5820 to 5875 cm^{-1}, we studied the behavior of these lines in a magnetic field.

A. Fe_L1

The results for the sharp Fe_L1 line at 5824 cm^{-1} are presented in Fig. 2, for **B** along the three crystal directions [001], [110], and [111]. The line splits isotropically into two

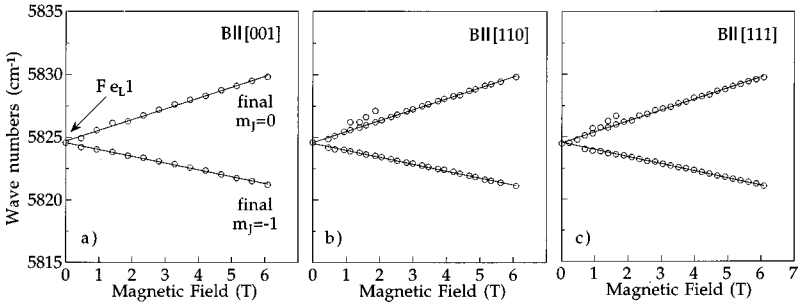

FIG. 2. Experimental Zeeman splitting of the Fe_L1 line for $\mathbf{B}\|[001]$, $\mathbf{B}\|[110]$, and $\mathbf{B}\|[111]$. The *g* value of the final state is derived from the splitting of the components.

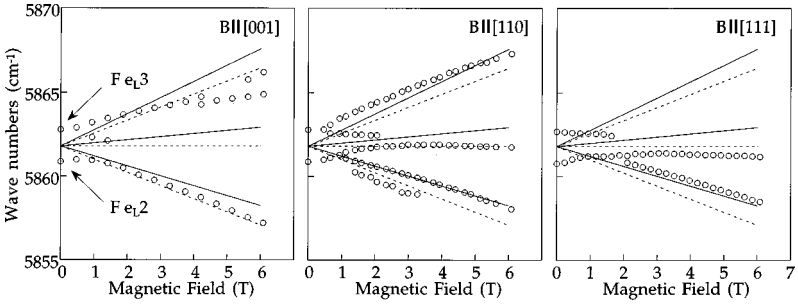

FIG. 3. Experimental Zeeman splitting of the Fe_L2 and Fe_L3 lines for $\mathbf{B}\|[001]$, $\mathbf{B}\|[110]$, and $\mathbf{B}\|[111]$. The expected transitions from a $^3A_2$ initial state to a $J'=2$ level, neglecting the zero-field splitting and all couplings to other states, is indicated ($g_J=1.67$). Full lines represent transitions from $m_J=-1$ of $^3A_2$ to $m_J=-2$, -1, and 0 of $J'=2$, and dashed lines those from a thermally populated $m_J=0$ state of $^3A_2$ to $m_J=-1$, 0, and 1 of $J'=2$.

prominent lines, disregarding a weaker high-energy component. The final state of the transition can be written as $^{2S+1}\Gamma$, where Γ is an irreducible representation of T_d symmetry. If Γ were one of the representations A_1, A_2, or E, the Zeeman splitting would be determined entirely by the spin S, with a splitting between two adjacent components ($\Delta m_S=1$) given by $\Delta E=g_s\mu_B B$. Here, μ_B is the Bohr magneton, and g_s the spin g value ($g_s=2.0023$). The experiment shows a clearly larger splitting. Thus Γ must be of either T_1 or T_2 symmetry, and we associate an effective orbital momentum $L'=1$ with Γ. Spin-orbit interaction will couple the spin $\mathbf{S}$ to $\mathbf{L}'$, and split the term into multiplet levels with an effective total angular momentum $\mathbf{J}'=\mathbf{L}'+\mathbf{S}$. The Zeeman Hamiltonian can thus be written as

$$H_{\text{Zeeman}}=\mu_B\mathbf{B}(g_L\mathbf{L}'+g_s\mathbf{S})=\mu_B\mathbf{B}g_J\mathbf{J}', \tag{1}$$

where g_L is the orbital g value. The splitting of the line is then determined by $\Delta E=\Delta m_J g_J\mu_B B$, and the g_J value is obtained from experiment by further assuming $\Delta m_J=1$. From the data in Fig. 2, we deduce an average value of $g_J=3.05$. In the weak-field limit, when the Zeeman splitting is smaller than the spin-orbit splitting, we have, for g_J,[11]

$$g_J=\frac{1}{2J'(J'+1)}\{(g_L+g_s)J'(J'+1)+(g_L-g_s)[L'(L'+1)-S(S+1)]\}, \tag{2}$$

and this expression is used to find the possible combinations of S and J' that yield a g_J value close to the experimental value. Experimentally $g_L=-0.28$ was obtained for Fe^+ by EPR.[12] The analysis shows that only spin values $\geqslant\frac{3}{2}$ can give a g_J as high as the experimental value. We find that we are most likely dealing with transitions to a state with $J'=1$, $S=2$ and $L'=1$, i.e., a $J'=1$ state of a spin-orbit split $^5T_1$ or $^5T_2$ term for which Eq. (2) gives $g_J=3.14$ when $g_L=-0.28$.

According to this assumption, the state should split into three components, $m_J=0$, ±1, when a magnetic field is applied. The shift of the line associated with the $m_J=0$ component is thus expected to be determined by the initial-state shift. Annealing experiments indicate that these transitions occur at the same center as the donorlike transitions discussed above, and we therefore assume that also in the present case the initial state is a $^3A_2$ term. The initial state of the transition (at ~2 K) is the $m_J=-1$ component. If we then identify the component shifting upwards in energy in Fig. 2 as the transition to the final $m_J=0$ state, an average initial ground-state g value of 1.9 is found, close to the value of $g_{sA}=2.0699$ observed experimentally in EPR (Ref. 1) for Fe^0. Consequently, the component shifting downwards in energy is attributed to transitions to the $m_J=-1$ state. Finally, as transitions from an $m_J=-1$ initial state to an $m_J=1$ final state are forbidden, this model predicts two observable components in agreement with experiment.

For two directions of the magnetic field, shown in Figs. 2(b) and 2(c), however, we see an additional weak component shifting to higher energies, visible only at low fields. We attribute this line to transitions from a thermally populated level of the Zeeman-split initial ground state, i.e., from the $m_J=0$ component of $^3A_2$. The line shifts to higher energies, and therefore it must be due to transitions to the $m_J=1$ component of the $J'=1$ state. From the shift of this line we obtain an approximate value of $g_J=2.9$, which agrees well with the value of 3.05 obtained above. Thus, we have substantial evidence from annealing studies and Zeeman experiments that the Fe_L1 line is due to transitions from the $^3A_2$ ground term of Fe^0 to an excited state with $J'=1$ of a spin-orbit-split $^5T_1$ or $^5T_2$ term. Such transitions are spin forbidden, but may become observable if they couple to spin-allowed final states.

B. Fe_L2 and Fe_L3

Having assigned the line Fe_L1 to transitions to a $J'=1$ state, we also expect to find transitions to $J'=2$ and 3 states. The weakly split lines at 5860 cm^{-1}, Fe_L2 and Fe_L3, are likely candidates for transitions to the $J'=2$ state. This assignment is further justified by the fact that the energy difference between these split lines and the $J'=1$ line is approximately the same as that between the two lowest shallow-donor series associated with the $J'=\frac{1}{2}$ and $\frac{3}{2}$ states of the $^4T_1$ term. We will see that this is to be expected, when we consider spin-orbit interactions in Sec. VII. In T_d symmetry, a $J'=2$ state is further expected to split into components of E and T_2 symmetries, resulting in the experimentally observed Fe_L2 and Fe_L3 lines.

In Fig. 3, the Zeeman behavior of the Fe_L2 and Fe_L3 lines is shown for three directions of the magnetic field. In addition to experimental data, shown as circles, we indicate the expected Zeeman splitting of a $J'=2$ state (disregarding any splitting at zero field), where we have used a g_J value of

TABLE II. Experimental and calculated energy values of the four lines in the $^5T_1$ multiplet. The energies are given in wave numbers (cm^{-1}). ΔE is the energy difference between each state and the lowest level in the multiplet, and ΔE_{calc} is the energy derived from the analysis in Sec. VII.

Final state	Symmetry label	Energy	ΔE	ΔE_{calc}
Fe_L1	$J'=1$ (T_1)	5824.39	0	0
Fe_L2	$J'=2$ (E)	5860.77	36.38	36.6
Fe_L3	$J'=2$ (T_2)	5862.64	38.25	37.6
Fe_L4	$J'=3$ (A_2, T_1, or T_2)	5872.80	48.40	44.2, 47.7, 49.6

1.67, calculated from Eq. (2) by arbitrarily setting the small g_L value to zero. Full lines describe transitions from the $m_J=-1$ initial state of $^3A_2$ to $m_J=-2$, -1, and 0 of $J'=2$, while dashed lines represent transitions from the thermally populated $m_J=0$ initial state of $^3A_2$ to $m_J=-1$, 0, and 1 of $J'=2$. In contrast to this simple isotropic model, the experimental data show an anisotropic splitting, and only some of the expected transitions are visible. The fit is of course poor, especially for low fields, since we have neglected the zero-field splitting of the line. However, the overall splitting behavior is given rather well, considering the fact that all parameters used in the model were obtained from an analysis of the $J'=1$ transitions. For higher fields we note that the lines bend toward lower energies, probably due to coupling to states higher in energy.

We do not see any strong lines that could be due to transitions to $J'=3$, but a weak line 10 cm^{-1} above the split $J'=2$ line could possibly be attributed to such a transition.[5] This line splits in a magnetic field but the components become too weak to be traced. Further investigations have to be carried out to justify the labeling of the lines in Table II, where the energy of each transition is given.

The important question at this stage is whether we can construct a $^5T_1$ or a $^5T_2$ final state for the excitation of Fe^0. Assuming that we excite an electron from the t_2 state, as was the case for transitions to the shallow-donor states, we will be left with a $^4T_1$ core and an excited electron with spin $S=\frac{1}{2}$. If this electron interacts with the core, this will result in two terms with total spin $S=1$ and 2. For this coupling to be effective in separating the two terms, the excited electron should be rather localized. A possible candidate for this state is the shallow-donor $1s(A_1)$ state, but here strongly affected by the local impurity potential. This model thus naturally leads to $^3T_1$ and $^5T_1$ terms of which the $^5T_1$ term should be lowest according to Hund's rule.

Taking a different point of view, we can consider the atomic $4s$ state of iron. Calculations have shown[13] that this state gives rise to a sharp a_1 resonance due to the local impurity potential, lying just above the conduction-band minimum. Within the local-density approximation, a spin-unrestricted calculation could not decide whether the a_1 resonance leading to high total spin enters the band gap or not.

As mentioned above, transitions to the $^5T_1$ state are spin forbidden, while those to the $^3T_1$ state are allowed. A mixing of the $^5T_1$ and $^3T_1$ states could, however, make the $^5T_1$ transitions visible. Spin-orbit interaction within our configuration can be responsible for such a coupling. The spin-orbit operator will to lowest order only mix states with equal J values. Since $^3T_1$ only contains $J'=0$, 1, and 2, we do not expect to see any transitions to the $J'=3$ level. In summary, we are lead to assign the Fe_L1, Fe_L2, and Fe_L3 to transitions from the $^3A_2$ ground state of Fe^0 to different components of the $^5T_1$ multiplet.

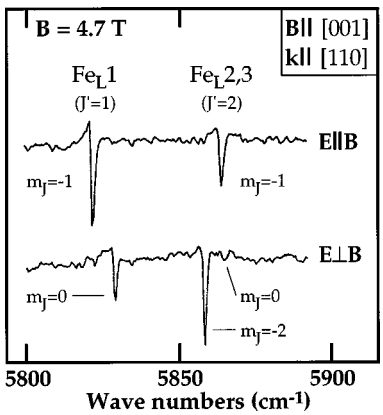

FIG. 4. Transmission spectra recorded with polarized light for $\mathbf{B}\|[001]$, showing the Zeeman split Fe_L1 ($J'=1$) and $Fe_L2,3$ ($J'=2$) spectral lines, for $\mathbf{E}\|\mathbf{B}$ and $\mathbf{E}\perp\mathbf{B}$. The peaks are labeled by the m_J value of the final state in the transition.

Ignoring for the time being that transitions from a $^3A_2$ ground state to a $S=2$ state are spin forbidden, and by considering the overall symmetry of the levels, we can in a first approximation determine which transitions in principle are symmetry allowed. The spin part of $^3A_2$ transforms as T_1, and combining this with the orbital A_2 symmetry, we have a T_2 initial state. Thus transitions to states with overall symmetry A_1, E, T_1, and T_2 are possible. The final states considered above have $J'=1$ and 2 which transform as T_1 and $E+T_2$, respectively. Figure 4 shows experimental spectra for the $J'=1$ (Fe_L1) and $J'=2$ ($Fe_L2,3$) lines obtained using polarized light and a pronounced polarization dependence is observed. If we neglect the weak zero-field splitting of the $J'=2$ line, regard m_J as a good quantum number, and only consider transitions from the lowest Zeeman-split component with $m_J=-1$ which transforms as $|T_2,-1\rangle$, a simple analysis of dipole-transition matrix elements yields selection rules that agree with the observed behavior.

VII. MULTIPLET SPLITTING OF $^4T_1$ AND $^5T_1$ STATES

When considering spin-orbit effects in the $^4T_1$ and $^5T_1$ terms discussed above, we note that all orbital contribution derives from the five electrons in the t_2 shell of Fe^+. The one-particle spin-orbit operator can be written

$$H_{so}^{e}=g_L\xi\mathbf{l}'\cdot\mathbf{s} \tag{3}$$

where ξ is the spin-orbit parameter, $\mathbf{l}'$ is the effective orbital momentum, $\mathbf{s}$ is the electron spin, and g_L is the orbital g value. Within a $^{2S+1}\Gamma$ term, the spin-orbit Hamiltonian is generalized to

$$H_{so}=g_L\sum_i \xi\mathbf{l}_i'\cdot\mathbf{s}_i=g_L\lambda\mathbf{L}'\cdot\mathbf{S}, \tag{4}$$

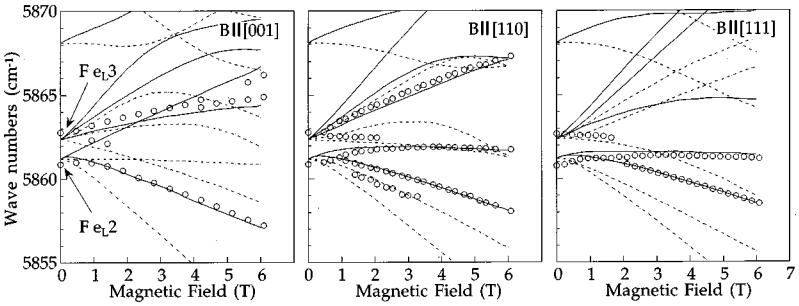

FIG. 5. The calculated Zeeman behavior of the $^5T_1$ term after parametrization of the $^4T_1$ and $^5T_1$ states. Full lines represent transitions from the $m_J=-1$ initial state, while dashed lines are due to transitions from the thermally populated $m_J=0$ state. Experimental data points are shown as circles.

where $\mathbf{L}'=\Sigma\mathbf{l}_i'$ is the total effective orbital angular momentum, $\mathbf{S}=\Sigma\mathbf{s}_i$ is the total spin, and λ the effective spin-orbit parameter. We expect both the $^4T_1$ and $^5T_1$ terms to have approximately the same g_L and ξ, since we assume that all orbital contribution derives from the t_2 shell of the core. In the following, we will use the EPR value[12] $g_L=-0.28$ for Fe^+.

For ground-state terms obeying Hund's rules, i.e., terms with maximum spin, one finds $\lambda=\pm\xi/(2S)$.[14] The plus and minus signs apply for less than or more than half-filled electron shells, respectively. Thus, for the $^4T_1$ state we have $\lambda[^4T_1]=-\xi/3$, and for the $^5T_1$ state $\lambda[^5T_1]=-\xi/4$. For the splitting between the two lowest spin-orbit split levels of $^4T_1$ and $^5T_1$ we find the same values

$$\Delta E[^4T_1]=E(J'=\tfrac{3}{2})-E(J'=\tfrac{1}{2})=\tfrac{3}{2}g_L\lambda[^4T_1]=-\tfrac{1}{2}g_L\xi,$$

$$\Delta E[^5T_1]=E(J'=2)-E(J'=1)=2g_L\lambda[^5T_1]=-\tfrac{1}{2}g_L\xi.$$

Experimentally we obtain $\Delta E[^4T_1]=42.13\ \mathrm{cm}^{-1}$ and $\Delta E[^5T_1]\approx 37\ \mathrm{cm}^{-1}$. We deduce approximate values of $\xi\approx 340\ \mathrm{cm}^{-1}$ ($^4T_1$) and $\xi\approx 300\ \mathrm{cm}^{-1}$ ($^5T_1$), which compare well with the free-ion value of the one-electron spin-orbit constant of 345 cm^{-1} given in Ref. 15. Our spherical model and the Landé interval rule predict that energies $E(J'=3)-E(J'=2)=\frac{3}{2}\Delta E[^5T_1]\approx 56\ \mathrm{cm}^{-1}$ and $E(J'=\frac{5}{2})-E(J'=\frac{1}{2})=\frac{5}{3}\Delta E[^4T_1]\approx 70\ \mathrm{cm}^{-1}$, which are considerably larger than the experimental values in Tables I and II. If the *C* and *D* series are in fact related to the split $J'=\frac{5}{2}$ level (Γ_7 and Γ_8), these states are strongly shifted toward lower energies. Also the $J'=2$ level of $^5T_1$ is split into two components (*E* and T_2). The weak component Fe_L4 could be assigned to a substantially shifted component of the $J'=3$ state, made visible by a possible higher order interaction.

The experimental results indicate that the lines we identify as transitions to the $^4T_1$ and $^5T_1$ states are closely correlated. We attribute the anomalies in multiplet line spacings and intensities[5] to the Fe^+ core, common to both final states. The core is essentially uncoupled from the excited shallow-donor-like electron in the $^4T_1$ case but couples to a rather more localized electron in an a_1 state via exchange interaction in the $^5T_1$ state. In order to correlate the two multiplet structures, we parametrize the observed splitting of the $^4T_1$ state using an effective Hamiltonian containing spin operators up to second order:[16]

$$H_{\mathrm{eff}}=\chi\mathbf{L}\cdot\mathbf{S}+K_1(\mathbf{L}\cdot\mathbf{S})^2+K_2(L_x^2S_x^2+L_y^2S_y^2+L_z^2S_z^2). \quad (5)$$

At this stage, the parametrization only serves as a way of summarily including all possible interactions with states higher in energy. The physical origin of these interactions is discussed briefly below. By diagonalizing H_{eff} in the $|T_1,S=\frac{3}{2},\mu,m_s\rangle$ basis of $^4T_1$, obtained as a direct product of the orbital $|T_1,\mu\rangle$ and spin $|S=\frac{3}{2},m_s\rangle$ functions, we recover the experimental energies of the $^4T_1$ multiplet with the parameters $\chi=6.92\ \mathrm{cm}^{-1}$, $K_1=-7.12\ \mathrm{cm}^{-1}$, and $K_2=3.02\ \mathrm{cm}^{-1}$. These parameters were obtained under the assumption that series *C* and *D* are associated with the Γ_7 and Γ_8 components of $J'=\frac{5}{2}$, respectively. It seems likely that the weaker series *C* involves Γ_7 and this relative ordering of Γ_7 and Γ_8 is in fact required to yield the observed ordering of the *E* and T_2 levels of $J'=2(^5T_1)$ below. In order to determine the $^5T_1$ levels we couple the $|T_1,S=\frac{3}{2},\mu,m_s\rangle$ states with an additional a_1 electron with $s=\frac{1}{2}$ and use Clebsch-Gordan coefficients to obtain the states $|T_1,S=1,\mu,m_s\rangle$ and $|T_1,S=2,\mu,m_s\rangle$, corresponding to $^3T_1$ and $^5T_1$ terms, respectively. From the matrix of H_{eff} in the $^4T_1$ basis, we determine by this transformation the matrix of H_{eff} in the ($^3T_1$, $^5T_1$) basis. If we now assume a sufficiently large exchange splitting between $^3T_1$ and $^5T_1$, matrix elements coupling the two terms may be neglected. By diagonalizing the $^5T_1$ submatrix we finally obtain the relative energies for the $^5T_1$ levels in terms of the parameters characterizing the $^4T_1$ term. These energies not only reproduce the experimental energy spacings among the $J'=1$ and 2 (*E* below T_2) levels of $^5T_1$ to within an accuracy of 1 cm^{-1}, but also confirm that the tentatively assigned Fe_L4 may be a component of the $J'=3$ level; see Table II.

The Zeeman behavior of the $^5T_1$ and $^3T_1$ multiplets can now be calculated by adding the matrix elements of the Zeeman Hamiltonian [Eq. (1)] to the ($^3T_1$, $^5T_1$) matrix of H_{eff}. The result is shown in Fig. 5 for the split $J'=2$ level of $^5T_1$. The full lines in Fig. 5 are associated with the $m_J=-1$ $^3A_2$ initial state, while dashed lines correspond to a thermally populated $m_J=0$ initial state. The calculated pattern is in good agreement with experimental data, shown as circles. This agreement can only be obtained if *E* lies below T_2. We will use the same set of parameters when we treat the Zeeman splitting of the $^4T_1$ core of Fe^+, discussed in Sec. VIII.

Since the spacing of the broad lines *R*1 and *R*2 agrees approximately with the experimental energy difference between the lowest levels of both the $^4T_1$ and $^5T_1$ multiplets,

we have considered the possibility that these features might be due to transitions to the $^3T_1$ multiplet. If this were the case, we would expect, in line with the findings for the $^4T_1$ multiplet, that the highest $J'=2$ level would have strongly reduced intensity and be shifted toward lower energies, close to the $J'=1$ level. From the multiplet splitting within $^3T_1$, obtained in the calculation above, we find that $R1$ might involve transitions to the $J'=0$ level and $R2$ transitions to both the $J'=1$ level and the nearby components of the $J'=2$ level. However, this raises the question why these transitions are so much broader than the sharp $^5T_1$ transitions. As the expected Zeeman splitting is small compared to the linewidth, no Zeeman effect could be resolved, which made it impossible to confirm any such assignment.

VIII. ZEEMAN EFFECT OF THE SHALLOW DONORLIKE TRANSITIONS

A. Initial state and Fe^+ core

The Zeeman effect causes the ground state $^3A_2$ of Fe^0 to split into three components ($m_J=0,\pm1$), where each component shifts by $\Delta E=m_J g_J \mu_B B$ with $g_J=g_{sA}=2.0699$. Since all measurements were carried out at temperatures below 2 K, we assume the thermal population of the $m_J=0$ and 1 states to be negligible (at least at higher fields) and thus the $m_J=-1$ state is the initial state in the transitions, transforming as $|T_2,-1\rangle$.

In order to analyze the possible transitions, we initially limit ourselves to a simple first-order treatment where we neglect all nonspherical effects. In the excitation process a t_2 electron is excited to a shallow-donor-like state. The two electrons in the e state remain unaffected by the transition, and retain their spin symmetry of $|T_1,-1\rangle$, while the five remaining electrons in the t_2 shell have total spin $S=\frac{1}{2}$ (spin-up and spin-down are denoted α and β, respectively) and orbital symmetry T_2. Coupling $S=1(e^2)$ and $S=\frac{1}{2}(t_2^5)$ to a high-spin configuration results in $S=\frac{3}{2}$ spin functions transforming as Γ_8 in T_d symmetry, which can be written down using Griffith's tables in Ref. 17 as

$$|\Gamma_8\kappa\rangle=|T_1,1\rangle\alpha,\quad m_S=\tfrac{3}{2},$$

$$|\Gamma_8\lambda\rangle=\sqrt{\tfrac{2}{3}}|T_1,0\rangle\alpha+\sqrt{\tfrac{1}{3}}|T_1,1\rangle\beta,\quad m_S=\tfrac{1}{2},$$

$$|\Gamma_8\mu\rangle=\sqrt{\tfrac{1}{3}}|T_1,-1\rangle\alpha+\sqrt{\tfrac{2}{3}}|T_1,0\rangle\beta,\quad m_S=-\tfrac{1}{2},$$

$$|\Gamma_8\nu\rangle=|T_1,-1\rangle\beta,\quad m_S=-\tfrac{3}{2}. \tag{6}$$

Coupling the total spin $S=\frac{3}{2}$ of the $^4T_1$ core with its orbital T_1 symmetry, we obtain the following expressions[17] for the components of the $J'=\frac{1}{2}$ level with Γ_6 symmetry which are involved in the transition series labeled A:

$$|\Gamma_6\alpha'\rangle=\sqrt{\tfrac{1}{2}}|T_1,-1\rangle|\Gamma_8\kappa\rangle-\sqrt{\tfrac{1}{3}}|T_1,0\rangle|\Gamma_8\lambda\rangle+\sqrt{\tfrac{1}{6}}|T_1,1\rangle|\Gamma_8\mu\rangle,\quad m_J=\tfrac{1}{2}, \tag{7}$$

$$|\Gamma_6\beta'\rangle=\sqrt{\tfrac{1}{6}}|T_1,-1\rangle|\Gamma_8\lambda\rangle-\sqrt{\tfrac{1}{3}}|T_1,0\rangle|\Gamma_8\mu\rangle+\sqrt{\tfrac{1}{2}}|T_1,1\rangle|\Gamma_8\nu\rangle,\quad m_J=-\tfrac{1}{2}.$$

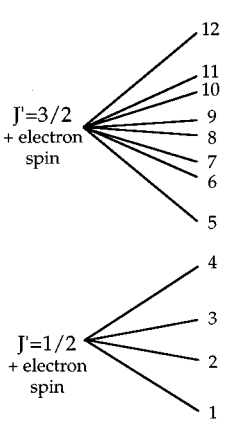

final core state	initial state of excited electron: orbital symmetry	initial state of excited electron: spin state	relative transition probability
12 $\|\Gamma_8,\kappa>$	—	α	0
11 $\|\Gamma_8,\lambda>$	—	α	0
10 $\|\Gamma_8,\kappa>$	—	β	0
9 $\|\Gamma_8,\mu>$	$\|t_2,-1>$	α	2/5
8 $\|\Gamma_8,\lambda>$	$\|t_2,-1>$	β	8/45
7 $\|\Gamma_8,\nu>$	$\|t_2,0>$	α	3/5
6 $\|\Gamma_8,\mu>$	$\|t_2,0>$	β	1/45
5 $\|\Gamma_8,\nu>$	$\|t_2,1>$	β	2/15
4 $\|\Gamma_6,\alpha'>$	—	α	0
3 $\|\Gamma_6,\alpha'>$	$\|t_2,-1>$	β	1/18
2 $\|\Gamma_6,\beta'>$	$\|t_2,-1>$	α	1/2
1 $\|\Gamma_6,\beta'>$	$\|t_2,0>$	β	1/9

FIG. 6. Schematic Zeeman splitting of the $J'=\frac{1}{2}$ and $\frac{3}{2}$ levels of the $^4T_1$ core when the spin splitting of the excited electron is included. The symmetry of the core state reached in the transitions are given together with the spin state and the orbital symmetry of the initial state of the excited electron. The expected relative probability ratios of each transition are derived from Eqs. (6) and (7).

Similar expressions for the $J'=\frac{3}{2}$ and $\frac{5}{2}$ levels can easily be written down.[17] We note that only the $|\Gamma_8\mu\rangle$ and the $|\Gamma_8\nu\rangle$ spin functions in Eq. (6) contain terms with $|T_1,-1\rangle$ symmetry for the two e electrons, and thus represent the only two possible final spin states in the transitions if the e electrons remain unaffected in the excitation process. Further, when the excited electron has spin-up (leaving t_2^5 in β), the core is left in the $|\Gamma_8\nu\rangle$ spin state; when the electron has spin-down (leaving t_2^5 in α), the core is left in the $|\Gamma_8\mu\rangle$ spin state. In this way we can easily estimate the probability ratios for the transitions to the different final core states.

In a magnetic field, the $J'=\frac{1}{2}(\Gamma_6)$ level is split by $\Delta E=g_J\mu_B B$ and, for the moment only taking the spin-splitting of the excited electron, $\Delta E=g_s\mu_B B$, into account, each zero-field transition of the A series will in principle split into four components, as shown in Fig. 6. A possible additional orbital splitting of the excited shallow-donor states will be discussed below. In Fig. 6 the transitions are labeled from 1 to 4, and for each we give the final state of the core, the orbital symmetry and spin of the initial state of the excited electron, and the relative probability factors obtained from Eqs. (7) and (8) as discussed above. Transition 4 is found to be impossible if the initial state is the $m_J=-1$ component of $^3A_2$, and thus we expect three experimental components with approximate intensity ratios 2:9:1. From a similar analysis of the $J'=\frac{3}{2}$ core-state transitions (series B), we find that, of the eight conceivable final states, three correspond to impossible transitions and only two of the five remaining allowed transitions are estimated to be strong; see Fig. 6.

B. Shallow donor states

The linear and quadratic Zeeman effect of shallow-donor states in silicon has previously been studied within the framework of EMT.[9] To analyze the transitions at Fe^0 which involve shallow donor states, we use the accurate description of the orbital splitting of these states as obtained in Ref. 9.

C. Experimental results

When fitting our data we must take into account (i) the Zeeman shift of the $m_J=-1$ state of the $^3A_2$ initial state, (ii)

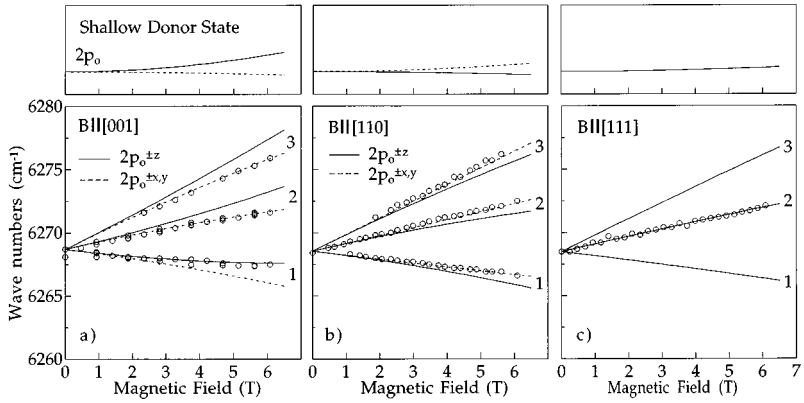

FIG. 7. Experimental Zeeman splitting of the $2p_0^A$ line for (a) $\mathbf{B}\|[001]$, (b) $\mathbf{B}\|[110]$, and (c) $\mathbf{B}\|[111]$. The predicted lines are labeled by the number of the final state of the core; see Fig. 6. In the top of the figure, the Zeeman splitting of a $2p_0$ shallow-donor state is given for comparison (Ref. 9).

the final-state $^4T_1$ core splitting, and (iii) the shallow-donor behavior as determined in Ref. 9. We will only consider the $2p_0$, $2p_\pm$, and $3p_0$ states of the two series involving the $J'=\frac{1}{2}$ and $\frac{3}{2}$ core states, i.e., the *A* and *B* series. The third and fourth series are too weak to be studied in a magnetic field. In all calculations of the $^4T_1$ core splitting below, the parametrization described in Sec. VII is used.

Figure 7 shows the Zeeman results for the $2p_0^A$ line with (a) $\mathbf{B}\|[001]$, (b) $\mathbf{B}\|[110]$, and (c) $\mathbf{B}\|[111]$. In Figs. 7(a) and 7(b), the dashed lines correspond to transitions to states at $\pm x$ and $\pm y$ valleys, while full lines are transitions to states at $\pm z$ valleys. In the insets above each figure, the corresponding theoretical splitting of a shallow $2p_0$ state is given[9] for comparison. The lines are labeled by numbers indicating the final state according to Fig. 6, which includes a specification of the Fe^+ core but only of the spin of the excited electron. The experimental data points closely follow the theoretical lines, but it is obvious that shallow-donor states belonging to different valleys are involved in the different transitions; i.e., for $\mathbf{B}\|[001]$, the $\pm z$ valleys are reached for line 1, whereas $\pm x$ and $\pm y$ valleys are reached for lines 2 and 3. For $\mathbf{B}\|[110]$, $\pm x$ and $\pm y$ valleys are reached regardless of the final state of the core. For $\mathbf{B}\|[111]$ there will be no splitting, since all valley orientations now are equivalent with respect to the direction of $\mathbf{B}$.

In order to interpret the experimental results of Fig. 7 we must consider the transformation properties of the shallow-donor states in somewhat greater detail. A p_0 state contains valley combinations of symmetries A_1, E, and T_2 at zero magnetic field, and transitions to all these combinations are symmetry allowed. The quadratic Zeeman shift of a p_0 state depends on the angle between the magnetic-field direction and its valley axis. The T_2 combinations, behaving as *x*, *y*, and *z* close to the origin, only involve valleys along the same axis, and remain eigenstates when the Zeeman Hamiltonian is included. The A_1 and E components, on the other hand, in general involve inequivalent valleys and may be mixed by the magnetic field. For *p* states we expect valley-orbit interactions to be negligible, and we may thus instead of A_1 and E consider combinations of valley states transforming as x^2, y^2, or z^2 associated with the $\pm x$, $\pm y$, or $\pm z$ valleys, respectively. These combinations are labeled (A_1E) combinations. Consider now, e.g., the transition corresponding to line 1 in Fig. 7(a), with $\mathbf{B}\|[001]$. The core is left in $|\Gamma_6\beta'\rangle$ (cf. Fig. 6) and the initial state of the excited electron has spin down and orbital symmetry $|t_2,0\rangle$, i.e., transforms as *z* and/or *xy*. With the electric field E parallel to the magnetic field ($\mathbf{E}\|\mathbf{B}\|\mathbf{z}$), only the p_0 state combination transforming as z^2 is observed, i.e., that (A_1E) combination involving $\pm z$ valleys. No transitions to p_0 states at *x* and *y* valleys are seen in this case. For $\mathbf{E}\perp\mathbf{B}$, transitions to states transforming as *x* and *y*, i.e., the T_2 combinations of p_0 states at $\pm x$ and $\pm y$ valleys, are allowed. Experimental data in Fig. 7(a) show that only the transition to the (A_1E) combination is strong enough to be observed. Applying the same analysis to the other transitions for $\mathbf{B}\|[001]$ and to those for $\mathbf{B}\|[110]$, we conclude that for all transitions to p_0 states those to the (A_1E) combinations are the strongest. Transitions to T_2 combinations have in fact not been clearly identified. Experiments using polarized light confirm the results of the above analysis. For $\mathbf{B}\|[111]$ no valley splittings occur, and for this particular sample only transitions corresponding to line 2 were sufficiently intense to be detected.

Forming the (A_1E) and T_2 combinations above actually implies multiplying a p_0 envelope function with a properly symmetrized linear combination of Bloch waves from the corresponding valleys. For, e.g., the x^2 combinations of (A_1E), this linear combination will contain a factor $\sin(k_x x)$, while for the *x* combination of T_2 the corresponding factor is $\cos(k_x x)$, where k_x is the Bloch vector of the *x* valley. The $\cos(k_x x)$ term significantly reduces the amplitude of the wave function at the four nearest-neighbor sites compared to the $\sin(k_x x)$ term, which may in part explain the experimental observations.

Figure 8 shows the experimental and calculated Zeeman behavior of the line complex $2p_\pm^A$, $2p_0^B$, and $3p_0^A$ for $\mathbf{B}\|[001]$. A manifold of lines is expected, but only a few of these correspond to transitions with sufficiently high transition probabilities to be detected experimentally. Lines expected to be weak, based on the results of Fig. 7, are, for clarity, omitted in Fig. 8; see the discussion below. We expect the $2p_\pm^{\pm z}$ states to split by $e\hbar B/m_t$, while the $2p_\pm^{\pm x,\pm y}$ states only show a small second-order split as they couple to $3p_0^{\pm x,\pm y}$. Each of the corresponding final states splits into three components due to the Zeeman splitting of the core and

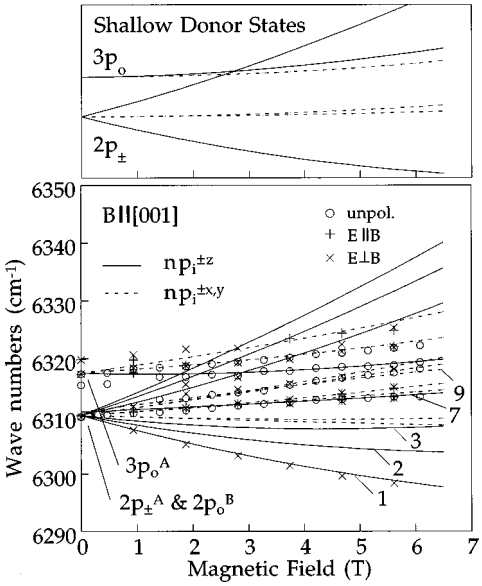

FIG. 8. Experimental and predicted Zeeman behavior of the $2p_{\pm}^{A}$, $2p_{0}^{B}$, and $3p_{0}^{A}$ lines for $\mathbf{B}\|[001]$; see text for details. Experimental data are marked as ○ for unpolarized light, + for $\mathbf{E}\|\mathbf{B}$, and × for $\mathbf{E}\|\mathbf{B}$. The transitions that are predicted to have high transition probabilities are shown as full and dashed lines, corresponding to transitions to shallow states at $\pm z$ and $\pm x, \pm y$ valleys, respectively.

the spin of the excited electron. The $2p_{\pm}^{A}$ lines are labeled by the final state of the core (1–3), according to Fig. 6. Solid lines mark transitions to shallow states at $\pm z$ valleys, and dashed lines those to $\pm x$ and $\pm y$ valleys. For the superimposed $2p_{0}^{B}$ line, only two final $J'=\frac{3}{2}$ core states are shown, corresponding to those transitions expected to be strongest, i.e., lines number 7 and 9 in Fig. 6. In addition to this core splitting, the $2p_{0}^{B}$ state splits due to the quadratic Zeeman effect, with $2p_{0}^{\pm z}$ states higher in energy than the $2p_{0}^{\pm x,\pm y}$ states, according to the results for the $2p_{0}^{A}$ state in Fig. 7(a).

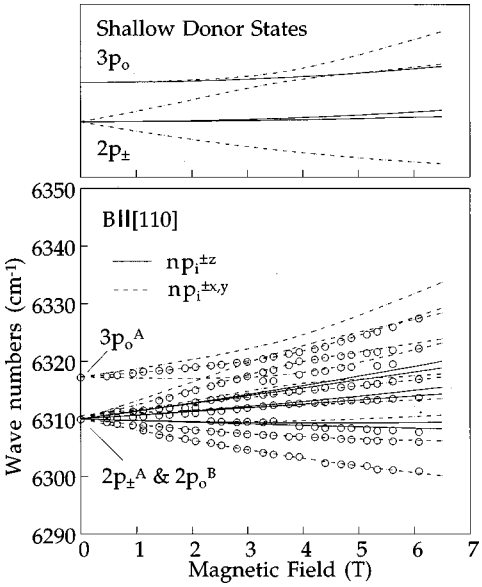

FIG. 9. Experimental data and theoretical behavior of the $2p_{\pm}^{A}$, $2p_{0}^{B}$, and $3p_{0}^{A}$ states for $\mathbf{B}\|[110]$.

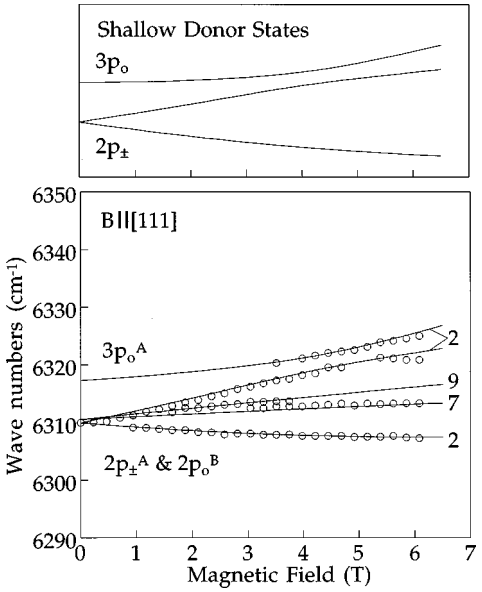

FIG. 10. Experimental data and theoretical behavior of the $2p_{\pm}^{A}$, $2p_{0}^{B}$, and $3p_{0}^{A}$ states for $\mathbf{B}\|[111]$. Only transitions to core-state numbers 2, 7, and 9 are indicated.

We assume that the results obtained for the intensities of the $2p_{0}^{A}$ components in Fig. 7 are applicable to all np_0 states in the spectrum. Transitions to $3p_{0}^{\pm z}$ states for line 1 and $3p_{0}^{\pm x,\pm y}$ states for lines 2 and 3 are therefore expected to be most prominent. For line numbers 7 and 9 of the $2p_{0}^{B}$ line, the initial state of the excited electron has orbital symmetries $|t_2,0\rangle$ and $|t_2,-1\rangle$, respectively, similar to lines 1 and 2 in the A series. We therefore expect transitions to $2p_{0}^{\pm z}$ states to be strongest for line 7, while for line 9 transitions to $2p_{0}^{\pm x,\pm y}$ states are expected to be strongest. Experimental data points are given in Fig. 8 for unpolarized light (○), for $\mathbf{E}\|\mathbf{B}$ (+), and $\mathbf{E}\perp\mathbf{B}$ (×). The fact that some transitions are observed only for polarized light is due to the weak intensity of the spectral lines.

Figure 9 shows the results for the same line complex, now with $\mathbf{B}\|[110]$. The information from Fig. 7(b) that transitions to $2p_{0}^{\pm x,\pm y}$ are strongest, no matter what core state is reached, is used for the $2p_{0}^{B}$ and $3p_{0}^{A}$ states, and only the

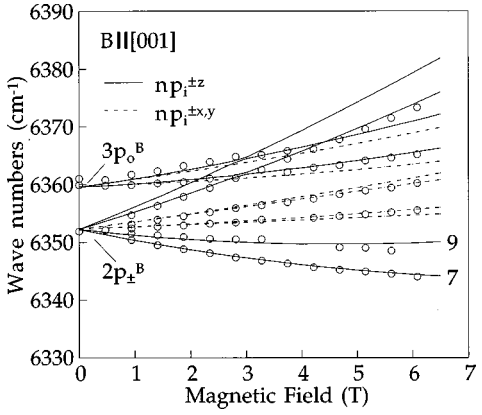

FIG. 11. Experimental data and theoretical behavior of the $2p_{\pm}^{B}$ and $3p_{0}^{B}$ states for $\mathbf{B}\|[001]$. Transitions to core-state numbers 7 and 9 are indicated.

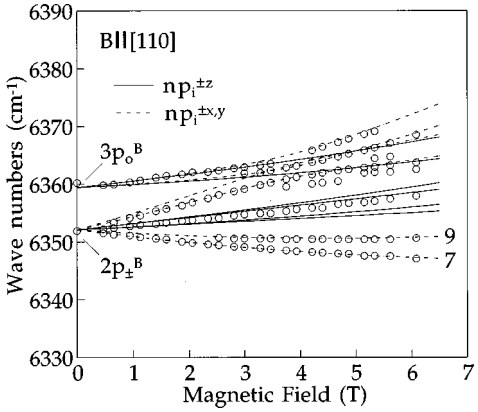

FIG. 12. Experimental data and theoretical behavior of the $2p_{\pm}^{B}$ and $3p_{0}^{B}$ states for $\mathbf{B}\|[110]$.

strongest theoretical transitions are included in the figure. For the $2p_{\pm}^{A}$ state, no transitions can be ruled out, and all possible lines are marked together with the experimental data points, corresponding to unpolarized light. The characteristic avoided crossing behavior between $2p_{+}^{\pm x,\pm y}$ and $3p_{0}^{\pm x,\pm y}$ is clearly observed.

Figure 10 shows the experimental and theoretical results for $\mathbf{B}\|[111]$. Since all valleys lie at the same angle to the magnetic field, the splitting pattern is less complex. Due to the low concentration of Fe_i^0 centers in this sample, only transitions with very strong intensity could be detected. In Fig. 10 we therefore only show the theoretical lines corresponding to transitions to one of the final core states of the *A* series, i.e., core state number 2, and two for the *B* series, core state numbers 7 and 9.

Figures 11 and 12 show the Zeeman behavior of the $2p_{\pm}^{B}$ and $3p_{0}^{B}$ states for $\mathbf{B}\|[001]$ and $\mathbf{B}\|[110]$, respectively, together with the theoretically predicted lines corresponding to core states 7 and 9. The agreement is excellent and justifies our assignment of the *B* series.

The almost perfect agreement between experimental results and our model for the *A* and *B* series supports our interpretation that the initial state of the transitions is the $^3A_2$ $m_J=-1$ component of Fe^0, and the final states are the $J'=\frac{1}{2}$ and $\frac{3}{2}$ states of the spin-orbit-split $^4T_1$ state, with the excited electron in a shallow donor state. Due to the low intensity of the transitions to what we may presume to be the split $J'=\frac{5}{2}$ state, and the fact that these states are expected to split into several even weaker components in a magnetic field, the assignment of the *C* and *D* series could not as convincingly be verified by Zeeman experiments. Those components, however, that were observed followed the predicted behavior satisfactorily.

IX. NON-LANDÉ BEHAVIOR

Our analysis of the electronic structure of Fe^0 has led to a consistent interpretation of all available data, especially for the lower components of the $^4T_1$ and $^5T_1$ multiplets. For the highest components, the experimental evidence indicates large deviations from the Landé interval rule and a strong decrease in intensity.[5] Unfortunately, as the corresponding lines are very weak, little detailed information on their behavior in a magnetic field or under uniaxial stress is available. Thus, very little conclusive evidence is available to determine what mechanism is responsible for this ''abnormal'' behavior. The simplest explanation would be a second-order spin-orbit coupling to electronic terms higher in energy. Although the electronic structure of these higher states is rather uncertain, an inspection of the relevant matrix elements shows that it is unlikely that this could be a dominating effect. In particular, it would be difficult to explain the strong modification of the highest component in view of the fact, that the lower components are well understood within our model. A much more natural explanation is based on the Jahn-Teller (JT) effect, and for many systems it has been shown that a dynamical JT interaction strongly modifies energy spacings and intensities.[18,19]

X. CONCLUSIONS

The ground and excited states of Fe^0 have been studied by means of high-resolution Fourier transform spectroscopy combined with a magnetic field. The analysis confirms that the ground state of Fe^0 has $^3A_2$ symmetry, and that two different kinds of excited states are observed. The first arises when an electron is excited to a shallow-donor-like state, close to the conduction band. The excited electron is delocalized and does not interact with the Fe^+ core, which is left in a $^4T_1$ state, i.e., a state with an effective angular momentum $L'=1$ and spin $S=\frac{3}{2}$. This state is experimentally found to split into four components, as four series of shallow-donor-like states are detected. The behavior of the Fe^+ core differs both in energy splittings and relative intensity from what is expected within a spherical model. First-order spin-orbit interaction causes the state to split into three components labeled $J'=\frac{1}{2}(\Gamma_6)$, $J'=\frac{3}{2}(\Gamma_8)$, and $J'=\frac{5}{2}(\Gamma_7+\Gamma_8)$. Experiment indicates that the $J'=\frac{5}{2}$ state splits into two components (Γ_7 below Γ_8), and that these components are strongly shifted toward lower energies in disagreement with the Landé interval rule. The experimental intensities for the transitions to $J'=\frac{3}{2}$ and $\frac{5}{2}$ are also much smaller than expected theoretically.

The second kind of excited state occurs when the electron is excited to a more localized *s*-like a_1 state which interacts with the $^4T_1$ core. This results in a $^5T_1$ term whose multiplet structure, when compared to Landé's interval rule, is found to be as distorted as that of the $^4T_1$ core. The first-order spin-orbit interaction splits the state into three components with $J'=1(T_1)$, $J'=2(E+T_2)$, and $J'=3(A_1+T_1+T_2)$. Experimentally, the $J'=2$ state is seen to split into two components, with the E state lowest in energy, and the $J'=3$ state is very weak in intensity and strongly shifted from its expected energy position.

The experimental observation of a significant deviation from Landé's interval rule for these two final-state multiplets suggests a substantial interaction either with higher electronic states or, what is more likely, with vibrational modes due to a dynamic Jahn-Teller distortion of the Fe_i center.

ACKNOWLEDGMENTS

The authors acknowledge financial support from the Swedish Natural Science Research Council (NFR) and the Swedish Research Council for Engineering Sciences (TFR).

[1] G. W. Ludwig and H. H. Woodbury, in *Solid State Physics*, edited by F. Seitz and D. Turnbull (Academic, New York, 1962), Vol. 13, p. 223; H. H. Woodbury and G. W. Ludwig, Phys. Rev. **117**, 102 (1960).

[2] G. G. DeLeo, G. D. Watkins, and W. B. Fowler, Phys. Rev. B **25**, 4962 (1982); **25**, 4972 (1982).

[3] A. Zunger, Solid State Phys. **39**, 275 (1987).

[4] H. Katayama-Yoshida and A. Zunger, Phys. Rev. B **31**, 7877 (1985); **31**, 8317 (1985).

[5] A. Thilderkvist, G. Grossmann, M. Kleverman, and H. G. Grimmeiss, Mater. Sci. Forum **143–147**, 165 (1994).

[6] J. Olajos, B. Bech Nielsen, M. Kleverman, P. Omling, P. Emanuelsson, and H. G. Grimmeiss, Appl. Phys. Lett. **53**, 2507 (1988).

[7] A. Thilderkvist, G. Grossmann, M. Kleverman, and H. G. Grimmeiss, in *Impurities, Defects and Diffusion in Semiconductors: Bulk and Layered Structures*, edited by O. J. Wolford, J. Bernholc, and E. E. Haller, MRS Symposia Proceedings No 163 (Materials Research Society, Pittsburgh, 1990), p. 51.

[8] A. Thilderkvist, M. Kleverman, G. Grossmann, and H. G. Grimmeiss, in *Proceedings of the 20th International Conference on The Physics of Semiconductors*, Thessaloniki (World Scientific, Singapore, 1991), Vol. 1, p. 581.

[9] A. Thilderkvist, M. Kleverman, G. Grossmann, and H. G. Grimmeiss, Phys. Rev. B **49**, 14 270 (1994).

[10] E. Janzén, R. Stedman, G. Grossmann, and H. G. Grimmeiss, Phys. Rev. B **29**, 1907 (1984).

[11] M. Tinkham, *Group Theory and Quantum Mechanics* (McGraw-Hill, New York, 1964).

[12] C. A. J. Ammerlaan and J. J. Van Kooten, in *Microscopic Identification of Electronic Defects in Semiconductors*, edited by M. M. Johnson, S. G. Bishop, and G. D. Watkins, MRS Symposia Proceedings No. 45 (Materials Research Society, Pittsburgh, 1985), p. 525.

[13] F. Beeler, O. K. Andersen, and M. Scheffler, Phys. Rev. B **41**, 1603 (1990).

[14] A. Abragam and B. Bleaney, *Electron Paramagnetic Resonance on Transition Metal Ions* (Dover, New York, 1986).

[15] T. M. Dunn, Trans. Faraday Soc. **57**, 1441 (1961).

[16] G. A. Slack, F. S. Ham, and R. M. Chrenko, Phys. Rev. **152**, 376 (1966).

[17] J. S. Griffith, *The Theory of Transition Metal Ions* (Cambridge University Press, London, 1961).

[18] W. Ulrici, in *The Dynamical Jahn-Teller Effect in Localized Systems* (North-Holland, Amsterdam, 1984).

[19] N. B. Manson and M. D. Sturge, Phys. Rev. B **22**, 2861 (1980).